Electroweak Measurements with the ATLAS and CMS Experiments

S. Hassani on behalf of the ATLAS and CMS Collaborations
DSM/IRFU (Institut de Recherches sur les Lois Fondamentales de l'Univers), CEA Saclay (Commissariat à l'Energie Atomique et aux Energies Alternatives), Gif-sur-Yvette, France

Various electroweak measurements have already been performed at ATLAS and CMS since the start of the LHC. These allow for precision tests of the electroweak dynamics of the Standard Model, but also challenge next-to-next-to-leading-order predictions. Differences between measurements and Standard Model predictions could prove evidence for new phenomena. A review of the latest results in W/Z and diboson physics is given. These consist of the measurement of the high-mass Drell-Yan differential and double-differential cross section, the study of the transverse momentum of the Z/γ^* using the ϕ^*_η variable and azimuthal correlations for events where a Z boson is produced in association with jets. Various diboson measurements are presented and measurements are in general found to be well described by the Standard Model predictions. These measurements test the non-Abelian gauge structure and limits on anomalous triple gauge couplings are derived, which are of impact comparable to the corresponding LEP and Tevatron results.

1 Introduction

Precision measurements of Drell-Yan lepton-pair production in pp collisions with the ATLAS [1] and CMS [2] detectors at the LHC will be presented. Measurements of production cross sections and associated angular correlations can provide unique insight into perturbative QCD in the absence of colour flow between initial and final states, the $V - A$ nature of the interactions, as well as enhance the knowledge of parton distribution functions in the proton. It also is an important source of Standard Model background for other processes; particularly interesting is the search for new physics at high dilepton invariant mass.

Study of the production of a Z boson in association with jets provides a test of predictions from perturbative QCD for a process that represents a substantial background to many physics channels. Results are presented as a function of jet multiplicity, for inclusive and differential Z boson production. The measurement of angular correlations between the Z and the "leading" jet (the one with the largest p_T) is presented. The experimental results are corrected for detector effects, and can be compared directly with QCD models.

Measurements of vector boson pair production provide excellent tests of the electroweak sector of the Standard Model (SM). In the SM, Triple Gauge Couplings (TGC) are predicted at tree level only with charged bosons, while neutral ones are forbidden. The TGC vertex is completely fixed by the electroweak gauge structure and so a precise measurement of this vertex, through the analysis of diboson production, is essential to test the high energy behavior of electroweak interactions and to probe for possible new physics in the bosonic sector. Any deviation from gauge constraints can cause a significant enhancement in the production cross section at high diboson invariant mass due to anomalous triple gauge boson couplings (aTGC). Due to the wealth of results only some details of these measurements can be highlighted here.

2 Drell-Yan production

At hadron colliders, the Drell-Yan (DY) process proceeds at tree-level via the s-channel exchange of a virtual photon or Z boson. Theoretical calculations of the differential cross section $\mathrm{d}\sigma/\mathrm{d}M_{\ell^+\ell^-}$ and the double-differential cross section $\mathrm{d}^2\sigma/\mathrm{d}M_{\ell^+\ell^-}\mathrm{d}Y$ where $M_{\ell^+\ell^-}(\ell = e, \mu)$ is the dilepton invariant mass, and Y is the absolute value of the dilepton rapidity, are currently described by perturbative QCD (pQCD) calculations at next-to-next-to-leading order (NNLO). With a simple signature benefiting from a relatively small background, experimental measurements of these distributions therefore provide an excellent test of the predictions of pQCD within the Standard Model. These measurements have also the potential to constrain the parton distribution functions (PDFs), in particular for antiquarks at large x. In addition, DY lepton-pair production is a major source of background for various physics analyses, such as $t\bar{t}$ and diboson measurements, as well as for searches for new physics beyond the Standard Model, such as the production of high-mass dilepton resonances.

The differential cross section for DY lepton-pair production has been reported by the ATLAS [3] and CMS [4] collaborations. Using $L = 4.9\,\mathrm{fb}^{-1}$ of data from pp collisions at a centre-of-mass energy of $\sqrt{s} = 7\,\mathrm{TeV}$, the invariant mass distribution of electron pairs from DY production has been measured at ATLAS as illustrated in fig. 1 in the range $116 < m_{ee} < 1500$ GeV, for electrons with $p_T > 25$ GeV and $|\eta| < 2.5$. The MC predictions are consistent with the shape of the measured m_{ee} distribution. The predictions of the FEWZ 3.1 [5,6] framework using five PDF sets at NNLO have also been studied. The framework combines calculations at NNLO QCD with NLO electroweak corrections, to which LO photon-induced corrections and real W and Z emission in single-boson production have been added. The resulting predictions are consistent with the measured differential cross section for all PDFs considered.

The differential and double-differential cross section $\mathrm{d}^2\sigma/\mathrm{d}M\mathrm{d}Y$ in the dimuon channel have been measured by CMS using $L = 4.5\,\mathrm{fb}^{-1}$ of data at $\sqrt{s} = 7\,\mathrm{TeV}$. The measurements are performed over the mass range 20 GeV to 1500 GeV and absolute dimuon rapidity from 0 to 2.4. The differential cross section measurements shown in fig. 1 (right), are normalized to the Z-peak region (60 - 120 GeV) in order to reduce systematic uncertainties. The $\mathrm{d}^2\sigma/\mathrm{d}M\mathrm{d}Y$ measured in the dimuon bin $[20, 30]$ GeV is presented in fig. 2 (left) and is compared to the POWHEG [7] NLO prediction calculated with CT10 [8] PDFs and the NNLO theoretical predictions as computed with FEWZ using the MSTW2008 [9] PDFs. Significant differences between data, POWHEG NLO and FEWZ NNLO calculations are observed at low masses.

A measurement of angular correlations in Drell-Yan lepton pairs via the ϕ^*_η observable [10] is presented in fig. 2 (right) using $L = 4.6\,\mathrm{fb}^{-1}$ of data at $\sqrt{s} = 7\,\mathrm{TeV}$ with the ATLAS detector. This variable ϕ^*_η probes the same physics as the Z/γ^* boson transverse momentum with a better experimental resolution. The observable ϕ^*_η is defined as : $\phi^*_\eta \equiv \tan(\phi_{acop}/2)\sin(\theta^*_\eta)$, where $\phi_{acop} \equiv \pi - \Delta\phi$, $\Delta\phi$ being the azimuthal opening angle between the two leptons, and the angle θ^*_η is a measure of the scattering angle of the leptons with respect to the proton beam direction in the rest frame of the dilepton system.

Normalised differential cross sections as a function of ϕ^*_η are measured separately for electron and muon decay channels and are then combined for improved accuracy. The cross section is also measured double differentially as a function of ϕ^*_η for three independent bins of the Z boson rapidity. The results are compared to QCD calculations and to predictions from different Monte Carlo (MC) event generators. The data are reasonably well described by resummed QCD predictions combined with fixed-order perturbative QCD calculations. Some of the Monte Carlo event generators are also able to describe the data. The measurement precision is typically better by one order of magnitude than present theoretical uncertainties.

3 Z + jets production

The production of jets of particles in association with a Z boson at the LHC provides an important test of perturbative quantum chromodynamics. Such events also constitute a non-negligible

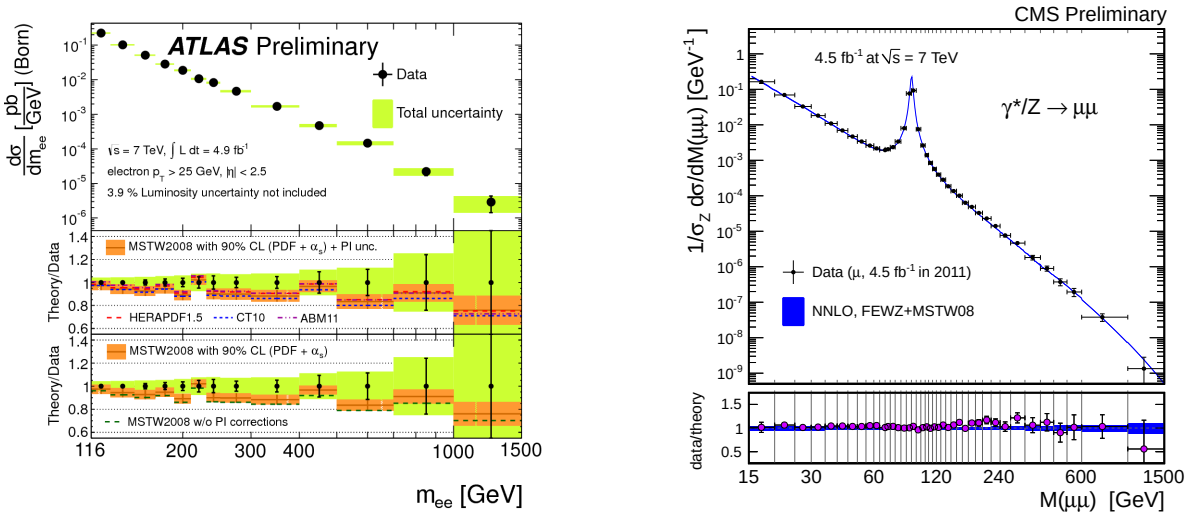

Figure 1: (Left) Measured differential cross section at the Born level with statistical and combined statistical and systematic uncertainties, excluding the 3.9% uncertainty on the luminosity. The measurement is compared to FEWZ 3.1 calculations at NNLO [3]. (Right) The Drell-Yan invariant mass spectrum, normalized to the Z resonance region, $r = 1/\sigma_{\ell\ell} \mathrm{d}\sigma/\mathrm{d}M$, as measured and as predicted by NNLO calculations, for the full phase space. The vertical error bar indicates the experimental (statistical and systematic) uncertainties summed in quadrature with the theory uncertainty resulting from the model-dependent kinematic distributions inside each bin in the dimuon channel [4].

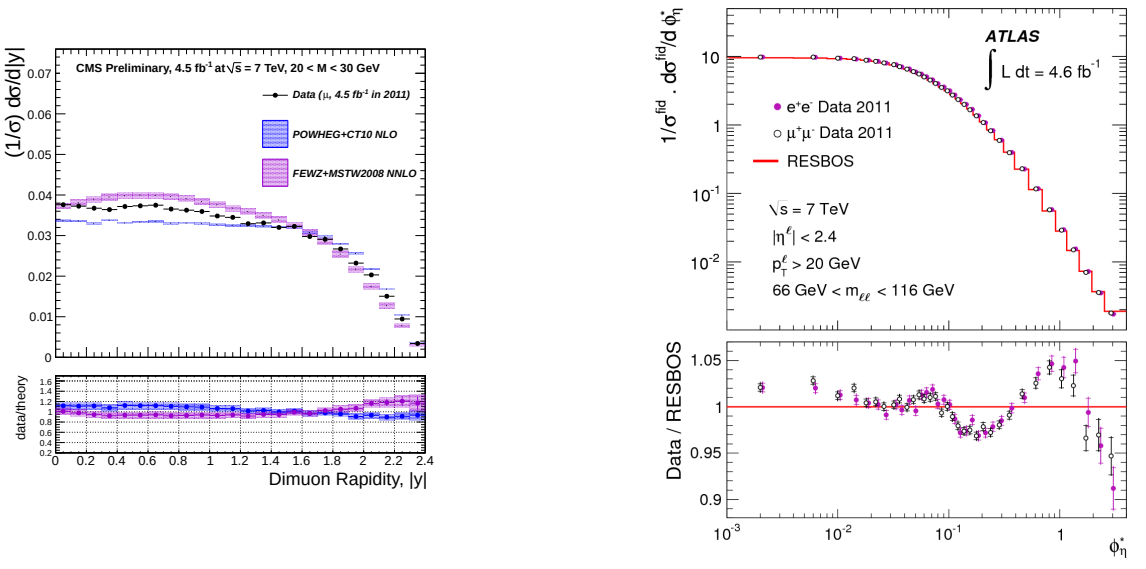

Figure 2: (Left) The Drell-Yan rapidity-invariant mass spectrum in detector acceptance in the dimuon channel, as measured and as predicted by NLO POWHEG+CT10 PDF and NNLO FEWZ+MSTW2008 PDF calculations. The error bands in the ratio plot combine the statistical, systematic and the PDF uncertainties [4]. (Right) The measured normalised differential cross section as a function of ϕ^*_η for $Z/\gamma^* \to e^+e^-$ (closed dots) and $Z/\gamma^* \to \mu^+\mu^-$ (open dots) channels [10]. The measurements are compared to ResBos [11] predictions represented by a line.

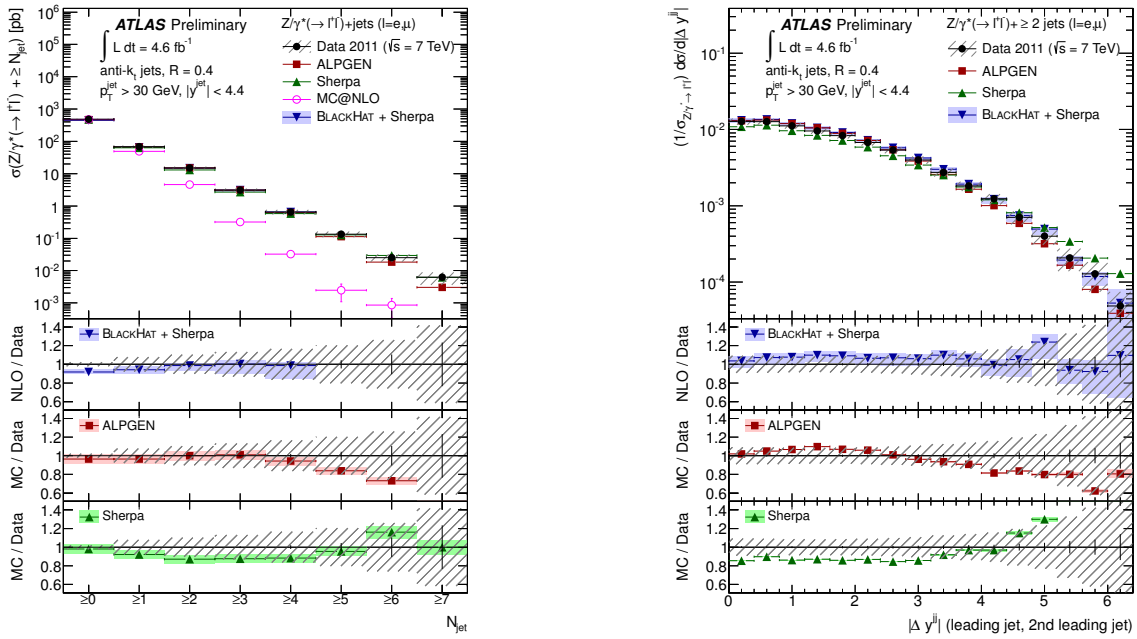

Figure 3: Measured cross section for $Z \to \ell\ell$ + jets as a function of the inclusive jet multiplicity (left) and the distance in rapidity between the two leading jets for events with at least two jets with $p_T > 30$ GeV and rapidity $|y| < 4.4$ in the final state (right). The error bars indicate the statistical uncertainty on the data, and the hatched (shaded) bands the statistical and systematic uncertainties on data (theory) added in quadrature [12].

background for studies of the Higgs boson candidate and searches for new phenomena.

Measurements of the production of jets of particles in association with a Z boson [12] have been preformed by ATLAS experiment using $L = 4.6\,\text{fb}^{-1}$ of data at $\sqrt{s} = 7$ TeV. Inclusive and differential jet cross sections in Z events, with Z decaying into e or μ pairs, are measured for jets with transverse momentum $p_T > 30$ GeV and rapidity $|y| < 4.4$. The data have been unfolded to the particle level and compared with predictions from ALPGEN [13] interfaced to HERWIG [14], Sherpa [15] and MC@NLO [16] generators and with fixed-order calculations from BlackHat [17] interfaced to Sherpa. Cross sections as a function of the inclusive and exclusive jet multiplicities and their ratios have been compared, as well as differential cross sections as a function of transverse momenta and rapidity of the jets and angular separation between the leading jets as shown in fig. 3. In general, the predictions of the matrix element plus parton shower generators and the fixed-order calculations are consistent with the measured values over a large kinematic range. MC@NLO fails to model higher jet multiplicities.

The measurement of angular correlations [18] between the Z and the "leading" jet (the one with the largest p_T), are based on data corresponding to $L = 4.6\,\text{fb}^{-1}$ collected with the CMS detector at $\sqrt{s} = 7\,\text{TeV}$. Figure 4 (left) shows the distributions for $Z \to \mu\mu$ candidate events in data, compared with expectations from simulated signal and background contributions using MADGRAPH [19] simulations normalized to the integrated luminosity of the data, as a function of associated jet multiplicity N_{jets}. Azimuthal correlations among the Z boson and the accompanying jets $\Delta\Phi(Z, \text{jets})$ are measured as functions of inclusive jet multiplicity ($N_{\text{jets}} \geq 1, \geq 2$, and ≥ 3) as shown in fig. 4 (right). The dominant sources of systematic uncertainty arise from uncertainties in jet-energy scale, resolution of jet p_T, background subtraction, and the unfolding procedure. Overall, the measured distributions are in agreement within uncertainties with the predictions from MADGRAPH. The predictions from SHERPA underestimate the measured distributions by about 10% whereas POWHEG predictions overestimate by about 10%. The disagreements with SHERPA and POWHEG become less pronounced at larger inclusive jet multiplicities.

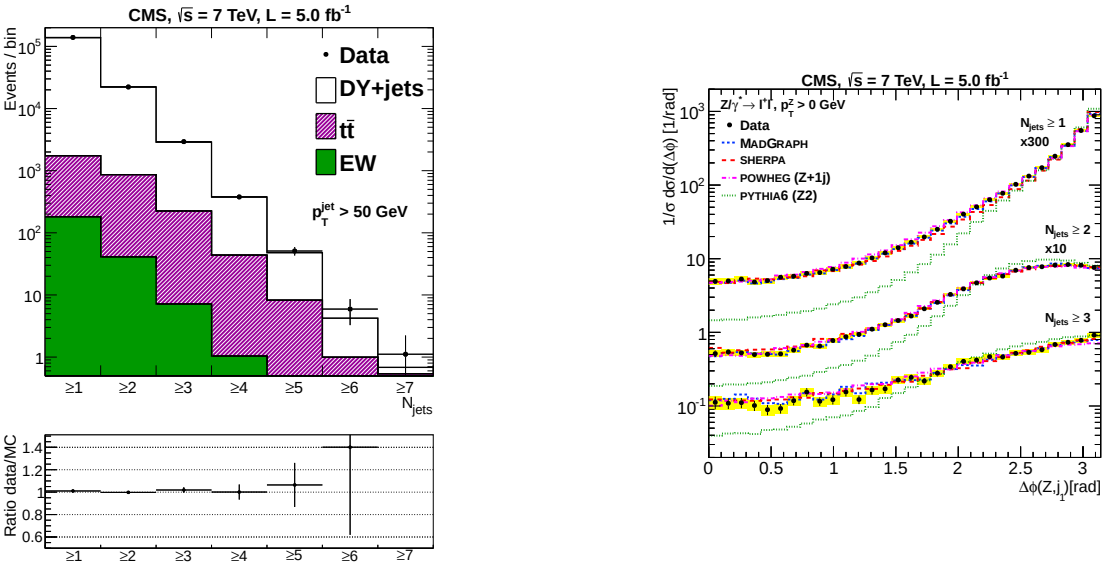

Figure 4: Distribution for $Z \to \mu\mu$ candidate events in data, compared with expectations from simulated signal and background contributions using MADGRAPH simulations normalized to the integrated luminosity of the data, as a function of associated jet multiplicity N_{jets} (left). Normalized $\Delta\Phi(Z, \text{jets})$ distributions for the leading jet in the inclusive jet-multiplicity bins ($N_{\text{jets}} \geq 1, \geq 2, \text{and} \geq 3$) (right) [18].

4 Diboson production and Triple Gauge Couplings measurements

The measurements of the diboson production cross sections and limits on aTGC were investigated by both ATLAS ans CMS experiments in the final states: $W\gamma, Z\gamma, WW, ZZ$ and WZ using 2011 data at a center-of-mass energy $\sqrt{s} = 7$ TeV and 2012 data at $\sqrt{s} = 8$ TeV. In the following, only the latest results prepared for this conference on WZ [20] and ZZ [21] analyses with 8 TeV data are reported.

4.1 ZZ cross section measurement

The analysis of Z boson pair production is performed in the $4l$ channel using $L = 20.3\,\text{fb}^{-1}$ of 2012 data at $\sqrt{s} = 8$ TeV with the ATLAS detector. The signature comprises of four isolated leptons with p_T above 7 GeV and the invariant mass of each reconstructed lepton pair is required to be in the mass window $[66, 116]$ GeV. The $4l$ final state is a very clean signature with small background contributions. These mainly come from Z+jets and $t\bar{t}$ processes where the jets are misidentified as leptons and they are estimated with data-driven methods. In the left plot of fig. 5 the mass of the leading lepton pair versus the mass of the sub-leading lepton pair, is given. After all event selections are applied, the observed yield in the $4l$ final state is 305 events with a background expectation of $20.4 \pm 2.9(stat.) \pm 5.0(syst.)$. The total cross section is $7.1^{+0.5}_{-0.4}(stat.) \pm 0.3(syst.) \pm 0.2(lumi.)$pb which is consistent with the Standard Model expectation of $7.2 \pm^{+0.3}_{-0.2}$ pb. Figure 5 (right) shows measurements of the total ZZ production cross section as a function of center-of-mass energy, from the ATLAS and the CMS experiments, and from the CDF and D0 experiments at the Tevatron, as well as the theoretical predictions.

4.2 WZ cross section measurement

The analysis of WZ production is performed with $3l\nu$ final states using $L = 13\,\text{fb}^{-1}$ of 2012 data at $\sqrt{s} = 8$ TeV with the ATLAS detector. The signature of these topologies is 3 high-p_T isolated leptons with $p_T > 15, 15, 20$ GeV for the two leptons from Z and the one from the W respectively, and $E_T^{miss} > 25$ GeV.

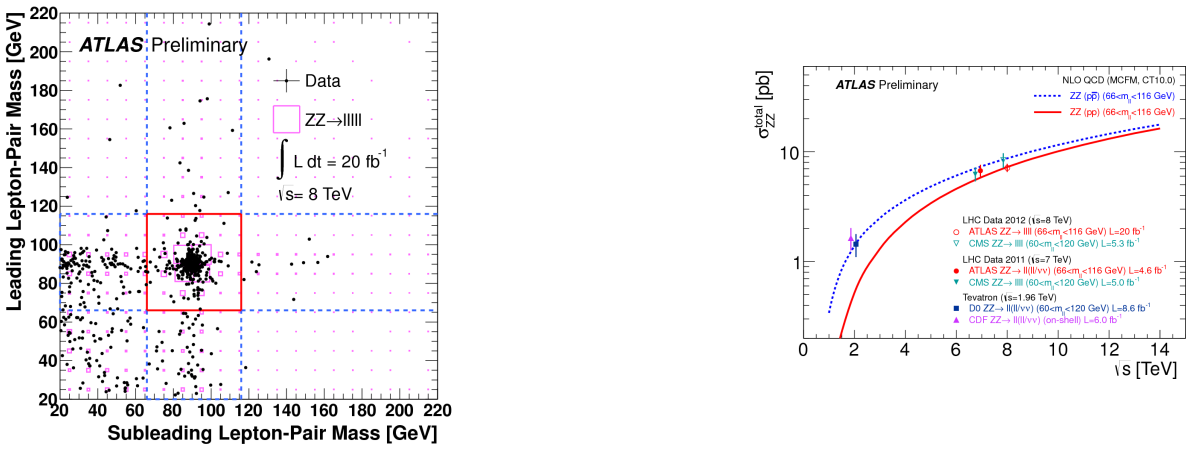

Figure 5: Left: The mass of the leading lepton pair versus the mass of the sub-leading lepton pair. The events observed in data are shown as solid circles and the $ZZ^* \to llll$ signal prediction from simulation as boxes. The size of each box is proportional to the number of events in each bin. The region enclosed by the solid (dashed) lines indicates the signal region defined by the requirements on the lepton-pair masses for ZZ (ZZ^*) events. Right: Measurements and theoretical predictions of the total ZZ production cross section as a function of center-of-mass energy $\sqrt{s}$. Experimental measurements from CDF and D0 in $p\bar{p}$ collisions at the Tevatron at $\sqrt{s} = 1.96\,\text{TeV}$, and experimental measurements from ATLAS and CMS in pp collisions at the LHC at $\sqrt{s} = 7\,\text{TeV}$ and $\sqrt{s} = 8\,\text{TeV}$ are shown. The blue dashed line shows the theoretical prediction for the ZZ production cross section in $p\bar{p}$ collisions. The solid red line shows the theoretical prediction for the ZZ production cross section in pp collisions [21].

Main sources of background are the Z+jets and $t\bar{t}$ events where the two leptons from the vector boson decays are accompanied by a jet which is misidentified as a lepton. These backgrounds are estimated from data-driven techniques. There is also a contribution from ZZ background events where one lepton falls outside the acceptance of the detector and thus creates E_T^{miss}. This source is estimated from MC. In fig. 6 (left), the E_T^{miss} is shown. The presence of three leptons in the final state and the requirement of a tight invariant mass window for the Z leptons around the Z pole ($|m_Z - m_{PDG}| < 10\,\text{GeV}$) suppresses significantly the background. Imposing stricter selection criteria for the W lepton with respect to the leptons coming from the Z boson, suppresses the background coming from Z+jets and $t\bar{t}$ even further. Given the selection requirements, the total number of observed events is 1094 with a background expectation of 277 ± 26 events. The measured total production cross section is $20.3^{+0.8}_{-0.7}(stat.)^{+1.2}_{-1.1}(syst.)^{+0.7}_{-0.6}(lumi.)$ pb while the expectation from SM is 20.3 ± 0.8 pb. Figure 6 (right) shows measurements of the total WZ production cross section as a function of center-of-mass energy, from the ATLAS

Figure 6: Left: Data and MC comparison of the E_T^{miss} distribution in trilepton events before applying the E_T^{miss} requirement. Right: Measurements and theoretical predictions of the total ZZ production cross section as a function of center-of-mass energy $\sqrt{s}$. Experimental measurements from CDF and D0 in $p\bar{p}$ collisions at the Tevatron at $\sqrt{s} = 1.96$ TeV, and experimental measurements from ATLAS in pp collisions at the LHC at $\sqrt{s} = 7$ TeV and $\sqrt{s} = 8$ TeV are shown. The blue dashed line shows the theoretical prediction for the WZ production cross section in $p\bar{p}$ collisions. The solid red line shows the theoretical prediction for the WZ production cross section in pp collisions [20].

Table 1: List of TGC parameters that enter in the effective Lagrangian for each diboson process.

interaction	parameters	channel
$WW\gamma$	λ_γ, $\Delta\kappa_\gamma$	WW, Wγ
WWZ	λ_Z, $\Delta\kappa_Z$,Δg_1^Z	WW, WZ
$ZZ\gamma$	h_3^Z, h_4^Z	Zγ
$Z\gamma\gamma$	h_3^γ, h_4^γ	Zγ
ZZZ	f_{40}^Z, f_{50}^Z	ZZ
$Z\gamma Z$	f_{40}^γ, f_{50}^γ	ZZ

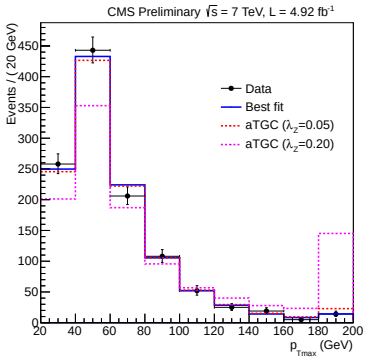

Figure 7: Leading lepton p_T distribution in WW channel, in data overlaid with predictions from the simulation with large anomalous couplings [24].

experiment, and from the CDF and D0 experiments at the Tevatron, as well as the theoretical predictions.

4.3 Triple Gauge Couplings measurements

The effect of aTGC is modelled using an effective Lagrangian which depends on the parameters [22,23] shown in table 1. If aTGCs exist they are expected to modify the production rates and kinematics of the processes which would manifest as enhanced production cross sections at high invariant mass and high-p_T as illustrated in figs. 7. Neutral aTGC are not allowed in the SM which predicts all parameters to be zero except for the charged aTGC parameters g_1^V and κ^V which are 1. In figs. 8 a summary of the limits set on the different aTGC parameters is shown along with comparisons to other experiments. These limits are set by the $W\gamma, WZ$ and WW and ZZ analyses described before. No deviation from the expected SM values is observed in any channel. TGC limits from WW analyses approach the precision of the combined limits from LEP experiments. Because of the higher energy and production cross section at the LHC, limits are better than the Tevatron. Limits from ZZ analyses are significantly tighter than the LEP and D0 experiments.

5 Summary

Results are presented for the measurements of the differential and double differential Drell-Yan cross section using the proton-proton collision data recorded with the ATLAS and CMS detectors at the LHC at $\sqrt{s} = 7\,\text{TeV}$. The measurements are compared to the predictions of perturbative QCD calculations at next-to-leading and next-to-next-to-leading order using various sets of parton distribution functions. Measurements of the production of jets of particles in association with a Z boson are presented. The data have been unfolded to the particle level and compared with predictions from different Monte Carlo generators implementing leading-order and next-to-leading order matrix elements supplemented by parton showers. Measurements of diboson cross sections have been performed with the ATLAS and CMS detectors at center-of-mass energy

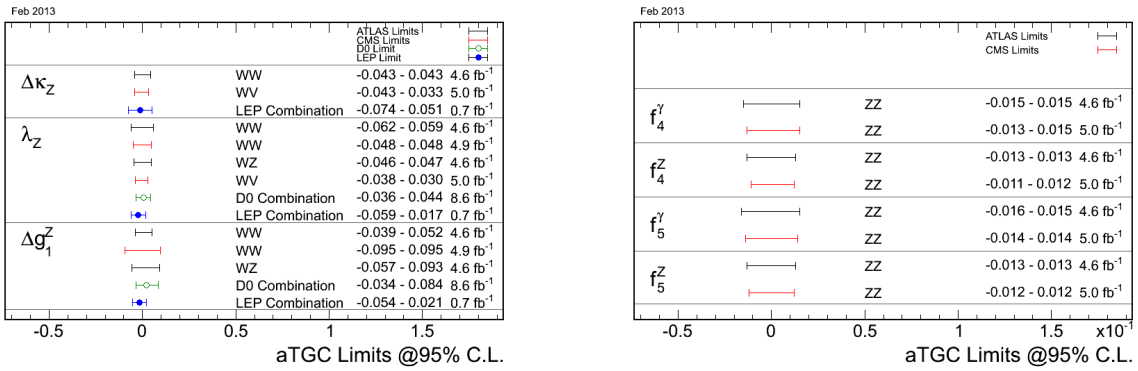

Figure 8: Left: 95% CL intervals for anomalous couplings from ATLAS, CMS, D0 and LEP for the charged aTGCs $\Delta\kappa_\gamma$ and λ_γ and Δg_1^Z. The ATLAS and CMS results from $W\gamma$, WW and WZ production are shown. The LEP charged aTGCs results were obtained from WW production, which is also sensitive to the WWZ couplings. The combined aTGC results from D0 were obtained from $WW + WZ \to l\nu jj$, $WW + WZ \to l\nu ll$, $W\gamma \to l\nu\gamma$ and $WW \to l\nu l\nu$ events. Except for the coupling under study, all other anomalous couplings are set to zero. Right: Neutral Anomalous TGC 95% confidence intervals from ATLAS and CMS experiments using ZZ events. The integrated luminosities are shown [25].

$\sqrt{s} = 7$ TeV with 2011 LHC data and at $\sqrt{s} = 8$ TeV with 2012 data. The total production cross sections are compatible with the SM expectations within uncertainties. No evidence for new physics is observed from the kinematic distributions of the diboson processes. Limits on anomalous triple gauge couplings are set in all channels and values of aTGC parameters are well within the SM predictions.

References

1. ATLAS Collaboration, *JINST* , 3 (2008)S08003.
2. CMS Collaboration, *JINST* , 3 (2008)S08004.
3. ATLAS Collaboration, ATLAS-CONF-2012-159, http://cdsweb.cern.ch/record/1493623.
4. CMS Collaboration, CMS-PAS-SMP-11-007.
5. K. Melnikov and F. Petriello, *Phys. Rev.* D **74**, 114017 (2006).
6. Y. Li and F. Petriello, *Phys. Rev.* D **86**, 094034 (2012)
7. S. Alioli et al., JHEP 07 (2008) 060, arXiv:0805.4802[hep-ph].
8. H.-L. Lai et al., *Phys. Rev.* D **82**, 074024 (2010), arXiv:1007.2241 [hep-ph].
9. A. D. Martin, W. J. Stirling, R. S. Thorne and G. Watt, Eur. Phys. J. C 63 (2009) 189.
10. ATLAS Collaboration, *Phys. Lett.* B **720**, 32-51 (2013).
11. F. Landry et al., *Phys. Rev.* D **67**, 073016 (2003), arXiv:hep-ph/0212159 [hep-ph].
12. ATLAS Collaboration, arXiv:1304.7098
13. M. Mangano et al., ALPGEN, JHEP 0307 (2003) 001, arXiv:hep-ph/0206293.
14. G. Corcella et al., JHEP 0101 (2001) 010, arXiv:hep-ph/0011363.
15. T. Gleisberg et al., JHEP 0902 (2009) 007, arXiv:0811.4622 [hep-ph].
16. S. Frixione and B. R. Webber, JHEP 0206 (2002) 029, arXiv:hep-ph/0204244.
17. H. Ita et al., arXiv:1108.2229 [hep-ph].
18. CMS Collaboration, arXiv:1301.1646.
19. J. Alwall et al., JHEP 1106(2011)128, arXiv:1106.0522 [hep-ph]
20. ATLAS Collaboration, ATLAS-CONF-2013-021, http://cdsweb.cern.ch/record/1525557.
21. ATLAS Collaboration, ATLAS-CONF-2013-020, http://cds.cern.ch/record/1525555.
22. K. Hagiwara et al., *Nucl. Phys.* B **B282**, 1987 (253).
23. J. Ellison et al., *Ann. Rev. Nucl. Part. Sci.* **48**, 1998 (33).
24. https://twiki.cern.ch/twiki/bin/view/CMSPublic/PhysicsResultsSMP12005.
25. https://twiki.cern.ch/twiki/bin/view/CMSPublic/PhysicsResultsSMPaTGC.